Large-scale piston error detection technology for segmented optical mirrors via convolutional neural networks

Dequan Li,[1,2,*] Shuyan Xu,[1] Dong Wang,[1] and Dejie Yan[1]

[1]Space Optics Department, Changchun Institute of Optics, Fine Mechanics and Physics, Chinese Academy of Sciences, Changchun, Jilin 130033, China
[2]University of Chinese Academy of Sciences, Beijing 100049, China
*Corresponding author: lidequan@ciomp.ac.cn

In the cophasing of the segmented optical mirrors, the Shack–Hartmann wavefront sensor is not sensitive to the submirror piston error and the large range piston errors beyond the cophasing detection range of phase diversity algorithm. It is necessary to introduce specific sensors (e.g., microlenses or prisms), but they greatly increase the complexity and manufacturing cost of the optical system. In this Letter, we introduce the convolutional neural network (CNN) to distinguish the piston error range of each submirror. To get rid of the dependence of the CNN dataset on the imaging target, we construct the feature vector by the in-focal and defocused images. The method surpasses the fundamental limit of the detection range by using different wavelengths. Finally, the results of the simulation experiment indicate that the method is effective.   © 2019 Optical Society of America

In order to pursue higher observation and resolution capabilities, telescopes have been developing in the direction of long focal length and large diameter in recent years [1]. The emergence of segmented telescopes greatly reduces the processing cost and the manufacturing cycle of the primary mirror. However, large-diameter telescopes composed of submirrors also face a series of technical challenges, the most difficult being the correction of the phase error between the submirrors which includes misalignments resulting from relative piston aberrations between segments and tip-tilt aberrations of each submirror [2].

Some methods proposed for cophasing segmented mirrors use a phase diversity (PD) algorithm [3], but the measurement range is limited. In Ref. [2], curvature sensors were first used for the piston detection. However, they lack ample capture range. Some methods use microlens [4] that must be aligned with high accuracy over each of the edges of the segments. We propose the PD algorithm to work jointly with the piston detector that is described in this Letter.

The method presented here makes use of the in-focal and defocused images at visible wavelengths, which is the same as

the PD algorithm, so no additional hardware is required. To get rid of the dependence of the training dataset on the imaging target, we construct the feature vector which is independent of the imaging content. An interferometric method cannot distinguish the differences in the number of waves away from the optical path lengths by monochromatic light. Through the use of combined wavelength and machine learning, the method described in this Letter can resolve this ambiguity.

The convolutional neural network (CNN) [5] is a deep learning model of multi-layer neuron connections. The model is constructed by the human visual system processing mechanism. The neurons shared by weights are convoluted on the input image to obtain features. The network can directly input the original image, avoiding complicated pre-processing of the image; thus, it is widely used. CNNs have been used in the past for cophasing optical segmented mirrors [6], but we build a new training method that does not depend on the imaging target of the optical system and can surpass the fundamental limit of 2π.

This Letter is organized as follows: the mathematical model of the problem is given. After that, the structure and training process of the CNN used in the Letter are explained. Then the construction of the training dataset and the simulation experiment are described. Finally, we present the conclusion and the future work.

The segmented type primary mirror system arranges a plurality of small-caliber optical components according to a certain spatial position, and adjusts each submirror to meet the confocal and cophasing requirement to achieve a single primary mirror of equivalent aperture optical performance.

This Letter refers to the primary mirror structure of the Keck telescope [7] and uses six hexagonal submirrors to form the primary mirror. The optical structure is shown in Fig. 1. The six submirrors are ring-shaped, and the middle is a light-passing hole. For convenience of description, each submirror is numbered one by one, and a coordinate system is established [8].

As shown in Fig. 1, the generalized pupil function of the segmented primary mirror can be written as

(a)   (b)
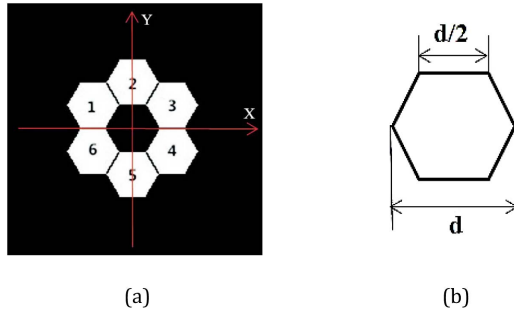
Fig. 1. Construction of the primary mirror and dimensions of the segmented sub-aperture.

$$P(x,y) = \sum_{j=1}^{N} P_j(x,y) \exp[i\phi_j(x,y)]. \tag{1}$$

p_j is the shape function of the jth submirror and can be given by

$$P_j = \begin{cases} 1 & \text{inside the } j\text{th hexagon} \\ 0 & \text{outside the } j\text{th hexagon} \end{cases}. \tag{2}$$

ϕ_j is the aberration corresponding to the jth submirror and can be expressed as a linear combination of Zernike polynomials. Only when considering the piston and tip-tilt aberration of each submirror, ϕ_j can be written as

$$\phi_j = \frac{2\pi}{\lambda}(\alpha_{j1}Z_{j1} + \alpha_{j2}Z_{j2} + \alpha_{j3}Z_{j3}). \tag{3}$$

In the above equation, Z_{j1} is the piston error of the jth submirror along the optical axis, Z_{j2} and Z_{j3} are the tip-tilt error of the jth mirror in the X-axis and the Y-axis, and a_{jn} are the corresponding aberration coefficients. The generalized pupil function of the segmented primary mirror can be written as

$$P(x,y) = \sum_{j=1}^{N} P_j(x,y) \exp\left[i\frac{2\pi}{\lambda}(\alpha_{j1}Z_{j1} + \alpha_{j2}Z_{j2} + \alpha_{j3}Z_{j3})\right]. \tag{4}$$

The relations of the focus image collected in the focus surface and the object in the spatial domain in this optical system are

$$i(x,y) = o(x,y) * \text{PSF}(x,y). \tag{5}$$

The relationship in the frequency domain is

$$I(u,v) = O(u,v) \cdot \text{OTF}(u,v). \tag{6}$$

In addition, $\text{PSF}(u,v)$ can be obtained by the inverse Fourier transform of a generalized pupil function:

$$\text{PSF}(u,v) = |\text{FT}^-(P(x,y))|^2. \tag{7}$$

In the above equation, the variables x, y are all variables in the spatial domain. $o(x,y)$ is the distribution functions of the two-dimensional object. $i(x,y)$ is the intensity distribution of the image on the ideal focal plane. $\text{PSF}(x,y)$ is the optical system point spread function corresponding to the intensity distribution of an ideal focal plane image. $P(x,y)$ is a generalized pupil function for an optical system. $\text{FT}^-(\ )$ is a two-dimensional inverse Fourier transform operation.

Similarly, the relations of the defocus image collected in the defocus surface and the object in the spatial domain in this optical system are

$$i_d(x,y) = o(x,y) * \text{PSF}_d(x,y). \tag{8}$$

The relationship in the frequency domain is

$$I_d(u,v) = O(u,v) \cdot \text{OTF}_d(u,v). \tag{9}$$

$$\text{PSF}_d(u,v) = |\text{FT}^-(P_d(x,y))|^2. \tag{10}$$

$$P_d(x,y) = A(x,y) \exp i(\phi(x,y) + \phi_d(x,y)). \tag{11}$$

In the above equation, $\phi_d(x,y)$ is the known defocus amount introduced which can be represented by the fourth term representing the defocus amount in the Zernike polynomial:

$$\phi_d(x,y) = a_4 c_4(\rho,\theta). \tag{12}$$

The network topology that was used is described. There are two convolutional layers (one pooling layer after each convolutional layer), two fully connected layers, and the last softmax output classification result. The structure of the used CNN is shown in Fig. 2.

The segmented mirror has a total of six submirrors, and the piston error range of each submirror is $[0, 10\lambda]$. If all the piston errors of the six submirrors are in the range of $[0, 1\lambda]$, and it is considered that the segmented mirror is in the cophasing range of PD, the work of the presented piston detector ends.

We use the first submirror as a benchmark; if the CNN is directly used to identify the piston error range of the five submirrors at the same time, the recognition step is λ. Then the identification type has 100,000 species, obviously this is impossible to achieve. Therefore, in this Letter, we train five CNNs with the same structure at the same time for identifying every submirror piston error, except the error of the first submirror; the identification type of every CNN has 10 species.

In this way, we can identify and correct the piston error of the submirrors to the cophasing range of PD. We repeat the above process until the piston errors of all the submirrors are corrected to $[0, 1\lambda]$; the specific operation flow of the algorithm is shown in Fig. 3.

If the in-focus image or the defocus image of the segmented mirror optical system with submirrors in different piston error ranges is directly used to construct the training dataset, the training dataset will be heavily dependent on the imaging target of the optical system, and different imaging targets will constitute different datasets however, in the actual situation, it is difficult to ensure that the imaging target is consistent with the imaging target that generates the training dataset. Therefore, the well-trained CNN will lose its meaning, so it is necessary to construct a simple training dataset which is not related to the imaging content.

Here we use the in-focus image and the defocus image of the segmented mirror optical system to form the CNN training set [9,10]:
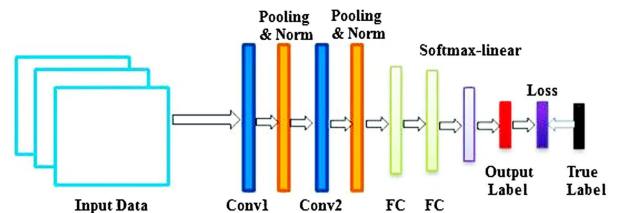
Fig. 2. Structure of the used CNN.
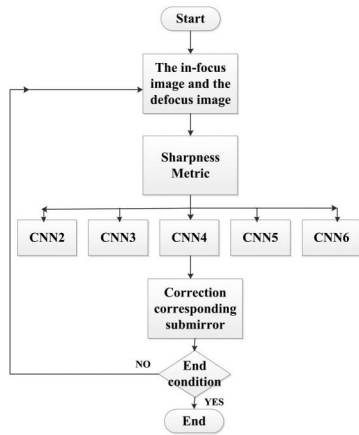
Fig. 3. Recognition flow of the submirror piston error.

$$M_{\text{sharpness}} = \frac{I \cdot I_d^* - I^* \cdot I_d}{I \cdot I^* + I_d \cdot I_d^*} = \frac{2iGG_d}{G^2 + G_d^2} \sin(\theta - \theta_d). \quad (13)$$

In the above equation, G is the amplitude of the in-focus image spectrum, G_d is the amplitude of the defocus image spectrum, θ is the argument angle of the in-focus image spectrum, θ_d is the argument angle of the defocus image spectrum, and $M_{\text{sharpness}}$ is the sharpness metric feature quantity represented by the in-focus image and the defocus image. It can be seen that this feature vector is independent of the imaging content. Table 1 is the in-focus image and the defocus image formed by the segmented mirror optical system for different targets and the corresponding sharpness metric feature quantity.

Table 1. In-Focus Image and the Defocus Image Formed by the Segmented Mirror Optical System for Different Targets and the Corresponding Sharpness Metric Feature Quantity

	Imaging 1	Imaging 2
Imaging Target		
In-Focus Image		
Defocus Image		
Sharpness Metric		

To surpass the fundamental limit of 2π in the detection range, a sequence of acquisitions with different wavelengths should be taken. In our example, we use $\lambda_1 = 700$ nm as the largest wavelength, and three additional shorter wavelengths $\lambda_2 = 0.93\lambda_1$, $\lambda_3 = 0.86\lambda_1$, and $\lambda_4 = 0.79\lambda_1$ to form a three-channel pseudo color image; three channels are used for three-channel training of the CNN.

The relevant parameters of the segmented active optics simulation system are as follows: the primary mirror consists of six hexagon submirrors; the effective apertures of the primary mirror D and submirror d are 4 and 1.46 m, respectively; the focal length is 40 m; the defocused length is set to 400 λ_1.

In order to better simulate the state of the segmented mirror in the cophasing, when the training dataset is generating, the tip-tilt aberrations of the six submirrors in the X-axis and Y-axis directions are seted in the range $[-0.5\lambda, 0.5\lambda]$, which are randomly generated by the MATLAB. There are 4000 training samples for every submirror; the range distribution is shown in Table 2.

After analysis and comparison in the simulation experiment, we find that the piston errors of each submirror interfered with each other seriously, which causes the CNN training to fail easily. Thus, we use statistical methods to find the data points in the $M_{\text{sharpness}}$ which are only sensitive to every submirror piston error. Below we present the data points for every submirror used in the $M_{\text{sharpness}}$ training dataset; see Table 3 for details.

We use TensorFlow to build the framework of the CNN; the network parameters are updated with a mini-batch gradient descent algorithm and the Adam update rule [11]. The size of the batch is 64, the number of the learning rate is 0.0001, and the maximum number of iterations is 10,000. In the training process of the CNN, we record the accuracy of the classification task every 50 iterations.

In Fig. 4, the accuracy of the every submirror piston error range classification task over training is plotted. As can be seen from Fig. 4, the final accuracy of the all submirror piston error range classification task over training attained is around 100%.

For each CNN, we build a test dataset of 160 samples that the network was not trained on. Every 16 test samples are randomly distributed in each piston error range. The recognition accuracy of each trained CNN over the test dataset is 97.5%, 98.1%, 98.7%, 98.1%, and 96.8%. The time of the trained CNN recognizes that a sample is about 0.91 s. The CPU we used is Intel(R) Core(Tm) i5-4460 K, and the frequency is 3.20 GHz; the graphics processing unit (GPU) we used is NVIDIA GeForce GT 730. The software version of Python

Table 2. Range Distribution of the $M_{\text{sharpness}}$ Training Dataset

Piston Error Range	The Number of Submirrors				
	2	3	4	5	6
$[0, \lambda]$	400	400	400	400	400
$[\lambda, 2\lambda]$	400	400	400	400	400
$[2\lambda, 3\lambda]$	400	400	400	400	400
$[3\lambda, 4\lambda]$	400	400	400	400	400
$[4\lambda, 5\lambda]$	400	400	400	400	400
$[5\lambda, 6\lambda]$	400	400	400	400	400
$[6\lambda, 7\lambda]$	400	400	400	400	400
$[7\lambda, 8\lambda]$	400	400	400	400	400
$[8\lambda, 9\lambda]$	400	400	400	400	400
$[9\lambda, 10\lambda]$	400	400	400	400	400

Table 3.   Typical Training Samples and the Training Data Points Used of Every Submirror

$M_{sharpness}$	Data Points Used of the Submirror 2	Data Points Used of the Submirror 3	Data Points Used of the Submirror 4	Data Points Used of the Submirror 5	Data Points Used of the Submirror 6
Piston Error Range of the Submirror	$[\lambda, 2\lambda]$	$[7\lambda, 8\lambda]$	$[6\lambda, 7\lambda]$	$[4\lambda, 5\lambda]$	$[\lambda, 2\lambda]$
The Number of Submirrors	2	3	4	5	6
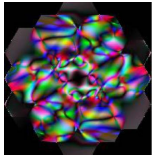
Fig. 4.   Accuracy of the every submirror piston error range classification task over training. In (a), the number of the submirror is 2. In (b), the number is 3. In (c), the number is 4. In (d), the number is 5. In (e), the number is 6.

is 3.5.2, and the software version of Tensorflow is tensor-flow_gpu-0.12.

It has been proven in this Letter that the method trained with simulated data is efficient. The piston error range of every submirror can be distinguished accurately, so we can calculate the remaining tip-tilt and piston value of segmented mirrors using the PD algorithm. The method is fast after the network is trained, and it requires no additional equipment by using the imaging camera of PD. It does not depend on the imaging target of the optical system and can surpass the fundamental limit of 2π in the detection range of the submirror piston error with the tip-tilt errors to $10\lambda_0$ by using combined wavelengths. However, there are some classification errors, and the method should be tested to be robust to the image noise; we will explore these problems further in future work.

REFERENCES

1. M. R. E. Lamont, Y. Okawachi, and A. L. Gaeta, Opt. Lett. **38**, 3478 (2013).
2. J. M. Rodriguez-Ramos and J. J. Fuensalida, *Optical Telescopes of Today and Tomorrow* (International Society for Optics and Photonics, 1997), Vol. **2871**, pp. 613–617.
3. D. Li, S. Xu, X. Qi, D. Wang, and X. Cao, Appl. Opt. **57**, 8212 (2018).
4. G. Chanan, C. Ohara, and M. Troy, Appl. Opt. **39**, 4706 (2000).
5. A. Krizhevsky, I. Sutskever, and G. E. Hinton, *ImageNet Classification with Deep Convolutional Neural Networks* (2012).
6. D. Guerra-Ramos, L. Díaz-García, J. Trujillo-Sevilla, and J. M. Rodríguez-Ramos, Opt. Lett. **43**, 4264 (2018).
7. G. Chanan, C. Ohara, and M. Troy, Appl. Opt. **39**, 4706 (2000).
8. Y. Dan, X. Shuyan, and N. Haitao, Appl. Opt. **54**, 7917 (2015).
9. R. L. Kendrick, D. S. Acton, and A. L. Duncan, Appl. Opt. **33**, 6533 (1994).
10. R. L. Kendrick, D. S. Acton, and A. L. Duncan, Proc. SPIE **2302**, 11 (1994).
11. D. P. Kingma and J. Ba, "Adam: a method for stochastic optimization," arXiv:1412.6980 (2014).